

Multi-Resolution Graph Analysis of Dynamic Brain Network for Classification of Alzheimer's Disease and Mild Cognitive Impairment

Ali Khazae¹, Abdolreza Mohammadi¹, Ruairi O'Reilly²

¹Department of Electrical Engineering, University of Bojnord

²Department of Computer Science, Munster Technological University

Abstract

Alzheimer's disease (AD) is a neurodegenerative disorder marked by memory loss and cognitive decline, making early detection vital for timely intervention. However, early diagnosis is challenging due to the heterogeneous presentation of symptoms. Resting-state functional magnetic resonance imaging (rs-fMRI) captures spontaneous brain activity and functional connectivity, which are known to be disrupted in AD and mild cognitive impairment (MCI). Traditional methods, such as Pearson's correlation, have been used to calculate association matrices, but these approaches often overlook the dynamic and non-stationary nature of brain activity. In this study, we introduce a novel method that integrates discrete wavelet transform (DWT) and graph theory to model the dynamic behavior of brain networks. Our approach captures the time-frequency representation of brain activity, allowing for a more nuanced analysis of the underlying network dynamics. Machine learning was employed to automate the discrimination of different stages of AD based on learned patterns from brain network at different frequency bands. We applied our method to a dataset of rs-fMRI images from the Alzheimer's Disease Neuroimaging Initiative (ADNI) database, demonstrating its potential as an early diagnostic tool for AD and for monitoring disease progression. Our statistical analysis identifies specific brain regions and connections that are affected in AD and MCI, at different frequency bands, offering deeper insights into the disease's impact on brain function.

Keywords: Resting-state functional magnetic resonance imaging; Alzheimer's disease; Graph theory; Discrete wavelet transform; Machine learning; False discovery rate analysis.

1- Introduction

Alzheimer's disease (AD) is a progressive neurodegenerative disorder that is characterized by memory loss and cognitive decline. Mild cognitive impairment (MCI) is an intermediate stage before early AD and individuals with MCI are at a heightened risk of progressing to AD [1, 2]. Currently, there is no known cure for AD, but various interventions, both pharmacological and nonpharmacological, have shown promise in slowing down its advancement, particularly when detected early [3, 4]. Therefore, accurate prediction of AD progression and differentiation between its stages are crucial for timely medical intervention [5]. Additionally, given the heterogeneity of symptoms in the initial stages of dementia among patients, identifying individuals at risk of progressing from MCI to early or late dementia poses a challenge [6].

Neuroimaging has had significant implications for the field of neuroscience. It has provided researchers with the ability to visualize brain activity, map neural networks, and investigate the underlying mechanisms of neurological disorders. Neuroimaging techniques help bridge the gap between neural activity and mental processes, leading to significant advancements in understanding brain-behavior relationships [7]. In addition to its impact on basic neuroscience research, neuroimaging plays a critical role in clinical applications. It has revolutionized the diagnosis and treatment of neurological and psychiatric disorders by enabling the identification of biomarkers, assessment of treatment response, and development of personalized therapies [8].

Among neuroimaging techniques, Magnetic Resonance Imaging (MRI) and Functional Magnetic Resonance Imaging (fMRI) play pivotal roles in the automatic classification of AD. While MRI focuses on anatomical structure, revealing brain regions affected by cortical atrophy and amyloid plaques, fMRI measures changes in blood flow and oxygenation, providing insights

into the brain's functional activity [9]. Specifically, resting-state fMRI (rs-fMRI) captures spontaneous brain activity and functional connectivity, which are disrupted in AD and MCI patients [5, 10, 11].

Most existing studies have used Pearson's correlation to calculate functional connectivity matrices, but this method fails to account for the dynamic nature of brain activity, resulting in a static representation that does not accurately reflect brain function. Some studies proposed sliding window methods to overcome this problem [12, 13], but these approaches have limitations, such as the use of fixed window sizes and the introduction of redundant information, which can bias the analysis and increase computational complexity. These drawbacks highlight the need for more sophisticated methods, such as wavelet analysis, which offers superior time-frequency localization and noise reduction.

The wavelet transform, a mathematical tool for decomposing signals into different frequency bands, has demonstrated its utility in various real-world applications [14, 15]. Despite the great potential of wavelet transform, it attracted little attention in neuroimaging. Recent studies have begun to explore its application, showing promising results in disorders like autism [16-18], depression [19, 20], ADHD [21], and Parkinson [22]. AD and MCI also have been investigated using wavelet transform in a few studies [23-25]. For example, Sadiq et al. [24] proposed a wavelet-based fractal analysis method that distinguished AD patients from healthy controls with an accuracy of 90.3%. These studies suggest that wavelet-based methods can effectively capture the complex dynamics of brain activity.

Our proposed method builds on this foundation by integrating discrete wavelet transform (DWT) with graph theory to model the dynamics of brain networks. Graph theory provides a robust

framework for analyzing complex networks, allowing us to represent and study the relationships between brain regions as a network of nodes and edges. Graph theory has been used previously to study brain network in AD [11, 26-30]. However, these studies ignored non-stationary nature of fMRI signals and have built their graphs based on the static functional connectivity matrices. By contrast, our approach constructs multiple graphs from DWT-decomposed rs-fMRI signals, capturing the brain's dynamic behavior across different frequency bands.

The novelty of our method lies in its multi-resolution representation of the dynamic brain network, which enhances the ability to discriminate between different stages of AD. By applying DWT, we analyze brain signals at multiple frequency bands, offering a comprehensive view of functional connectivity across different temporal scales. This multi-resolution approach enhances the ability to detect subtle changes and patterns that may indicate different stages of AD. The integration of graph theory allows us to extract meaningful measures that reveal the underlying structure of the brain's functional connectivity at various frequencies. Additionally, machine learning algorithms are employed to automate the classification of subjects based on these graph measures, enabling accurate identification of AD and MCI stages.

We evaluate our method using rs-fMRI data from the Alzheimer's Disease Neuroimaging Initiative (ADNI) database, demonstrating its potential as an early diagnostic tool and for monitoring disease progression. Performance metrics such as accuracy, sensitivity, and specificity are used to assess the method's effectiveness, while statistical analysis identifies key brain regions and connections affected in AD and MCI.

In summary, the integration of DWT, graph theory, and machine learning in our proposed method offers a novel and powerful approach to understanding and diagnosing AD. By capturing

the dynamic, multi-resolution nature of brain networks, our approach provides a more accurate and detailed representation of brain function, which could significantly improve the early detection and monitoring of Alzheimer's disease.

2- Methods

2-1- Subjects

This study will analyze rs-fMRI data of subjects from the Alzheimer's Disease Neuroimaging Initiative (ADNI) database (Table 1). The ADNI is a longitudinal multicenter study designed to develop clinical, imaging, genetic, and biochemical biomarkers for the early detection and tracking of AD. The ADNI database is a vast repository of data collected from over 10,000 participants, including MRI and PET images, genetics, cognitive tests, CSF and blood biomarkers, and clinical information. The data is available to authorized investigators through the Image Data Archive (IDA). It has been used to identify new biomarkers for AD, to develop diagnostic tools, and to study the progression of the disease. The database is also being used to develop new treatments for AD.

As a longitudinal database, it enables researchers to track the progression of AD and to investigate biomarkers that can be used to diagnose the disease early. The variety of data types available provides researchers with a comprehensive view of the disease and enables analysis from multiple angles. The Healthy control (HC), patients with AD, and patients with MCI will be selected based on the age, gender, and cognitive scores such as Mini-Mental State Examination (MMSE) and Clinical Dementia Rating (CDR) which indicate mild or moderate dementia.

2-2- Data acquisition and preprocessing

Functional and structural MRI data are collected according to the ADNI acquisition protocol using three tesla (3T) scanner [31]. The rs-fMRI data in each subject consisted of 140 functional volumes and acquired with following parameters: repetition time (TR) = 3000 ms; echo time (TE) = 30 ms; flip angle = 80°; slice thickness=3.313 mm; and 48 slices.

The standard preprocessing steps of rs-fMRI data will be performed. Briefly, the preprocessing steps are as follows: leaving the first few volumes (7 volumes) of the functional images for signal equilibrium and participant's adaptation to the circumstances; slice-timing correction to the last slice; realignment for head movement compensation by using a six-parameter rigid-body spatial transformation [32]; normalization to the Montreal Neurological Institute (MNI) space; resampling to 3-mm isotropic voxels; detrending; smoothing using a Gaussian filter with full width at half maximum (FWHM) of 4 mm; and band-pass filtering (0.01-0.08 Hz).

During the realignment step, four subjects (two normal, one MCI, and one AD) who exhibited head motions more than 2.5 mm of displacement and 2.5 degrees of rotation in any direction, were excluded. The whole-brain signal is removed by a multiple linear regression analysis to reduce the effect of the physiological artifacts [33-35]. To reduce the effects of motion and non-neuronal blood oxygen level-dependent (BOLD) fluctuations, head motion as well as the cerebrospinal fluid (CSF) and white matter signals are removed as nuisance covariates [33, 36]. Preprocessing is carried out using the Data Processing Assistant for Resting-State fMRI (DPARSF) toolbox [37] and the SPM (Statistical Parametric Mapping) package (<http://www.fil.ion.ucl.ac.uk/spm>).

2-3- Brain network analysis

2-3-1- Time series extraction

After preprocessing of the rs-fMRI images, the rs-fMRI signals of each voxel are extracted. The next step is to analyze these signals to identify patterns of functional connectivity between different brain regions. An initial choice is the voxel-based functional connectivity analysis. However, it has the drawback of high complexity due to the high number of voxels. Brain parcellation is used for dividing the brain into distinct regions or parcels and use them as region of interests (ROIs). There are two main types of brain parcellation methods.

Anatomical methods such as Automated Anatomical Labeling (AAL) and Talairach atlases are based on the physical structure of the brain. These methods use features such as cytoarchitecture, sulci, and gyri to define brain regions. Functional methods such as independent component analysis (ICA) are based on the functional activity of the brain. As we are studying brain function by rs-fMRI data, predefined functional brain atlases such as the 264 putative functional area atlas [38] are employed to parcellate the brain. The time series of voxels within each of ROI are averaged to generate a representative signal for each ROI.

2-3-2- Wavelet analysis

The DWT is a time-frequency analysis method that decomposes a signal into a series of wavelet coefficients. Wavelets are oscillatory functions that have a localized frequency content. This means that they can be used to represent signals that have a specific frequency content. One common way of DWT implementation is to use a filter bank. A filter bank is a set of filters that are designed to extract different frequency bands from a signal. The DWT can be implemented by

passing the signal through a filter bank and then calculating the coefficients of the resulting wavelet functions. The DWT has a number of advantages over other time-frequency analysis methods. One advantage is that it is a localized method. This means that the wavelet coefficients are only sensitive to a specific frequency band. This makes it a good choice for applications where it is important to preserve the details of the signal. Another advantage of the DWT is that it is a multiresolution method. This means that it can be used to decompose a signal into a hierarchy of levels. This can be useful for dynamic connectivity applications where it is important to analyze the signal at different levels of detail.

There are many different wavelet functions, but some of the most common ones include Haar, Daubechies, Morlet, Gabor, and Biorthogonal wavelet families. We will examine the different wavelet families at various degree and scales to find the optimal one. The DWT is used to decompose ROI signals in different levels. Association between the extracted rs-fMRI signals of ROIs is calculated using Pearson's correlation. This gives the original connectivity matrix. This procedure is repeated for decomposed rs-fMRI signals at different levels and result in frequency sub-band connectivity matrices.

2-3-3- Thresholding

As stated above, the original and frequency sub-band association matrices are constructed by calculation of Pearson's correlation of the corresponding signals of ROIs. The resulted association matrices are weighted dense connectivity matrices. Graph theory is a mathematical tool that is capable of concisely quantifying the properties of complex systems and modeling interrelationships (represented by edges) between brain regions (represented by nodes) and has

proved to be sensitive in digging network measures of psychiatric and neurological diseases [39]. Thus, graphs of original and frequency sub-band association matrices are constructed by setting each ROI as a node and correlation values as edges.

For further analysis, we converted the weighted dense connectivity to sparse ones by thresholding them at an optimal threshold value. We employ some methods to find an optimal value for threshold [40]. The binary undirected connectivity matrices for each subject are calculated by thresholding the connectivity matrices and setting their diagonal elements to zero.

2-4- Computation of graph measures

The binary undirected connectivity matrices for each subject are represented by corresponding graphs and used to calculate the various graph measures. The Brain Connectivity Toolbox (BCT) [41] is used to this end. The BCT is a comprehensive and widely used software package designed for analyzing and characterizing brain network connectivity using graph theory measures. It provides a collection of functions and algorithms that enable researchers to study the properties, organization, and dynamics of complex brain networks.

The provided measures can be categorized into several groups, including Node-Level Measures, Global Measures, Network Efficiency Measures, Modularity Measures, and Resilience Measures. These comprehensive set of measures capture all aspects of the brain network and reveal inherent information in different time-frequency layers.

Three measures of clustering coefficient [42], local efficiency [43], and ratio of local to global efficiency were computed to characterize the ability of the brain for specialized processing within densely interconnected groups of regions. Two measures of characteristic path length [42]

and global efficiency [43] were used to assess ability of the brain in rapidly combining specialized information from distributed regions. Nine measures of degree, node strength, participation coefficient [44], diversity coefficient [45], betweenness centrality [46], K-coreness centrality [47], subgraph centrality [48], eigenvector centrality [49], and PageRank centrality [50] were computed to investigate properties of different areas of brain. In addition, one measure of resilience (i.e. assortativity [51]) and one measure of network small-worldness [42, 52] were also computed. The above-mentioned graph measures were calculated based on the binary adjacency matrices. The last measure, node strength, was computed based on the weighted networks. These measures, together, construct the final feature vector for each normal, MCI, and AD subject. The size of final feature vector for each subject at each level of wavelet decomposition was 2909 ($11 \times 264 = 2904$ local and 5 global features).

2-5- Statistical Analysis

To determine the altered connectivity networks in AD and MCI patients, we analyzed raw connectivity matrices using False Discovery Rate (FDR) method implemented in NBS toolbox [53]. The FDR method controls the expected proportion of falsely rejected hypotheses, offering a more sensitive approach than traditional methods like Bonferroni, which tend to be conservative and have low power. It classifies voxels into four types based on true activity and declaration status, calculating the FDR as the ratio of false positives to the total number of declared active voxels. The FDR method automatically adjusts thresholds based on the strength of the signal, making it adaptive and suitable for different significance levels in neuroimaging studies. Its main application lies in neuroimaging data analysis, specifically in fMRI, where it helps determine

statistically significant results across all voxel-wise test statistics, providing a more effective and interpretable thresholding method compared to traditional approaches [54].

2-6- Feature Selection

An efficient feature selection algorithm is the essential part of a machine learning approach in case of high dimensional datasets, such as rs-fMRI. Feature selection stage selects an optimal subset of features from the original feature set. Feature selection facilitates data understanding, reduces the storage requirements and training-testing times, and improves accuracy of classification. Feature selection algorithms roughly divide into two categories: filter and wrapper methods. The filter methods select a subset of features according to the general characteristics of data, independently of chosen classifier. However, the wrapper methods require a predetermined classifier and evaluate features according to their performances in discrimination of classes. The Fisher algorithm and the sequential feature selection algorithm are the most popular filter and wrapper methods, respectively. These algorithms are explained briefly here.

Fisher score is a univariate filter method that is commonly employed to determine the discriminatory power of individual features between two classes of equal probability [55]. It is independent of the class distribution. Fisher score for each feature in a two class problem is defined as:

$$FS = \frac{n_1(m_1 - m)^2 + n_2(m_2 - m)^2}{(n_1\sigma_1^2 + n_2\sigma_2^2)} \quad (1)$$

where m is the mean value of the feature, m_1 and m_2 are feature mean values on each class, σ_1^2 and σ_2^2 are respective variances, and n_1 and n_2 are number of samples in two classes. Forward sequential feature selection (FSFS), starting from the empty set of features, sequentially adds feature that results in the highest objective function when combined with the features that have already been selected. Backward sequential feature selection works in the opposite direction of FSFS and starting from the full set, sequentially removes the feature that results in the smallest decrease in the value of the objective function.

2-7- Classification and performance metrics

In this study, supervised machine learning methods was used to construct the classifier. A set of input data, namely training dataset, was used to train the supervised machine learning algorithm and produce desired output. We used the support vector machine (SVM) and naïve Bayes classifier as the supervised machine learning algorithms. SVM is a supervised machine learning method that was originally developed for binary classification problems [56]. The classification algorithm was implemented in MATLAB (The Math Works, Natwick, MA) using LIBSVM software package (www.csie.ntu.edu.tw/~cjlin/libsvm/). The naïve Bayes classifier in its basic form assumes that features are conditionally independent within each class. This assumption simplifies the training step because the density can be calculated individually for each feature. The independence assumption is usually violated in practice, though it has been shown that the naïve Bayes classifier tolerates this violation [57-59]. In fact, there is not necessarily a relation between classification performance and fitting quality to a probability distribution. The

quality of fit to a probability distribution is related to the appropriateness of the independence assumption [60].

We have used holdout cross validation to train and test the classifier. Holdout method randomly selects K subjects from each group for training, leaving the others for testing. In this study, the value of K was set to 23. Therefore, number of training samples was 69 (23 from each group) and number of testing samples was 95 (20 Normal, 65 MCI, and 10 AD).

3- Results

3-1- Statistical analysis on raw connectivity matrix

The procedures used in this study for data processing and classification are shown in Figure 1. After pre-processing of the rs-fMRI data, the 264 putative functional areas were employed to parcellate the brain. Then signals of all voxels within each region were averaged to produce 264 signals for each subject. DWT was applied to each of the 264 extracted signals, and the approximate coefficients were computed for decomposition levels 1 through 5. As the result of this part of our proposed method, for each ROI, five DWT decomposed signals and one original signal were calculated. Pearson's correlation was applied on extracted signals to construct 264-by-264 connectivity matrices of the brain network graph. For each subject, one original connectivity matrix and five DWT decomposed connectivity matrices were produced. The above procedure repeated using 20 different wavelet types (db1, db2, ...) at five levels of decomposition. Finally, one original connectivity matrix and 100 DWT decomposed connectivity matrices were produced for each subject. Using the raw connectivity matrices of subjects at AD, MCI, and HC groups, we performed FDR analysis (an alternative method to correct for multiple comparisons) in 10,000

random permutations, to find disrupted connectivity patterns in patients with AD and MCI. FDR analysis gave us a sparse matrix of connections with significant differences between groups. Figure 2 shows the result for the original signals. The same figures (and corresponding sparse matrices of significant connections (edges)) were obtained by applying FDR analysis on connectivity matrices of different wavelet types and different levels of decomposition. Finally, we have 101 sparse matrices of connections with significant differences between three groups of HC, MCI, and AD. We wanted to find the most frequent significant edges (connections), at each level of decomposition. So, we accumulated disrupted connectivity matrices at each level of decomposition across all wavelet types. As the result, a matrix was resulted for each level of decomposition (Figures 3 to 7). The maximum weight of each connection was 20, for edges that were found significant at all FDR analysis on level i ($i= 1, 2, 3, 4,$ and 5) decomposed connectivity matrices using all wavelet types of db1, db2, Table 2 shows disrupted ROIs and connections (nodes and edges). Table 3 shows the significant nodes and connections when original rs-fMRI signals were used to construct connectivity matrices. It is noteworthy that this will result in only one sparse matrix of significant connections.

3-2- Application of machine learning approaches to graph measures

After the statistical analysis, we investigated whether graph measures can differentiate patients with AD and MCI from healthy subjects. To this end, we used the proposed method in Section 2-3-3 and found the optimal value of $P = 0.22$ for converting the raw connectivity matrices to the sparse networks. Then the graph measures were calculated for sparse brain networks. The calculated measures were used as discriminative features to classify three classes: normal control subjects, patients with MCI, and patients with AD. The number of graph nodes in this study was

264 and thus we calculated 264 features for each of the following measures: degree, node strength, participation coefficient, betweenness centrality, K-coreness centrality, subgraph centrality, eigenvector centrality, PageRank centrality, diversity coefficient, local efficiency, and ratio of local to global efficiency. In addition, we calculated one feature for the following global measures: average path length, average clustering coefficient, global efficiency, assortativity, and small-worldness. These features were combined to construct the final feature vector for each subject at each level of decomposition for each wavelet type. The size of final feature vector was 2909 ($11 \times 264 = 2904$ local and 5 global features). Performing the classification using this high dimensional feature space is time consuming and usually results in poor performance due to the existence of redundant and irrelevant features. Feature selection was performed on the extracted 2909 features to select the most informative features. Filter feature selection algorithms were used as a pre-processing step since they are simple and fast. We found that the Fisher algorithm provided the best results in the filtering stage. The filter feature selection algorithm (i.e. Fisher algorithm in this study) sorts the features based on their discrimination ability. The best feature is on the top of the list with maximum discrimination. Then, we added the FSFS wrapper stage after the filter stage. The FSFS was applied on the first half of the selected features from the filter stage to find the final features. Since the typical goal of classification is to maximize the accuracy, the FSFS feature selection procedure performs a sequential search using the accuracy of the learning algorithm on each candidate feature subset. The training set was used to select the features and to fit the model, and the test set was used to evaluate the performance of the final selected features. This procedure was repeated for features extracted using graph measures of connectivity matrices of different wavelet families at different levels of decomposition. Tables 4-7 show the

classification results using wavelet families of Coiflet, Daubechies, Fejér-Korovkin, and Symlet, respectively.

4- Discussions

Comparison of the dense connectivity matrix of the brain network of three groups (normal, MCI, and AD) using the FDR analysis revealed significant altered networks in patients with MCI and AD (Figures 2-7). An altered network with 17 nodes and 16 edges was found using FDR analysis on raw connectivity matrices obtained from original rs-fMRI signals (Figure 2). Half of the edges (8 connections) in the altered network were related to the regions in DMN. Six connections were between DMN and visual system and two connections were between DMN and dorsal attention system. From Table 2, the most affected nodes in FDR analysis using matrices of first level of decomposition were located in DMN, visual, uncertain, sensory/somatomotor hand, and dorsal attention, respectively. The affected regions of brain in FDR analysis of matrices from second level of decomposition were located in DMN, visual, uncertain, salience, and sensory/somatomotor hand, respectively. FDR analysis using third level of decomposition resulted in altered regions mostly located in uncertain, DMN, fronto/parietal task control, visual, and salience, respectively. Regions in DMN, fronto/parietal task control, uncertain, visual, and salience were found mostly affected during FDR analysis of connectivity matrices obtained from fourth level of decomposition. Most of altered nodes of FDR analysis of fifth level of decomposition were located in DMN, fronto/parietal task control, visual, salience, and sensory/somatomotor hand, respectively. Compared to the result of FDR analysis on connectivity matrix obtained from original rs-fMRI signals (Table 3): visual, DMN, uncertain, sensory/somatomotor hand, and dorsal attention are common resting state networks that have been affected mostly.

These results are in agreement with previous results which reported decreased connection strengths between the temporal lobe and the parietal and occipital regions [61]. The observation of functional disruption in regions within sensory/somatomotor (hand and mouth), DMN, dorsal attention, and visual are also in agreement with previous results [62-64].

The second column of Table 2 depicts the most frequent significant nodes across different wavelet types and levels of decomposition. Overall, across the all wavelet types and levels of decomposition, ROIs of 99, 26, 250, 64, 8, 38, 156, 159, 12, 154, 225, 192, 5, and 147 from 264 putative functional area atlas were among most frequent disrupted areas due to the AD and MCI. These ROIs correspond to the areas in AAL atlas which located in Angular_L, Temporal_Inf_R, Temporal_Mid_L, Temporal_Pole_Sup_L, Occipital_Inf_L, Occipital_Mid_L, Occipital_Mid_L, Lingual_L, Occipital_Inf_L, Precentral_R, Frontal_Mid_Orb_L, Fusiform_L, and Temporal_Mid_R. **Angular_L**: The angular gyrus is part of the DMN, which is often disrupted in AD. Studies have consistently reported decreased functional connectivity in the angular gyrus among AD patients, which correlates with impairments in episodic memory and language processing [65-67]. The left angular gyrus (ROI 99 of 264 putative functional area atlas in Table 2) was found as a disrupted region in most cases of our experiments. Interestingly, in a recent study [67], the left angular gyrus was highlighted as a critical region where atrophy leads to disturbed neural dynamics in the DMN, resulting in cognitive impairment, particularly in attention-related symptoms. The findings suggest the left angular gyrus could be a potential target for non-invasive brain stimulation techniques to slow or modify Alzheimer's disease symptoms. Repetitive transcranial magnetic stimulation (rTMS) has shown beneficial effects, with potential applications to modulate atypical DMN brain dynamics [67]. **Temporal_Inf_R, Temporal_Mid_L, Temporal_Mid_R (ROIs 26, 250, 147)**: The temporal lobes, including the inferior and middle

temporal gyri, are critical for memory and semantic processing. Decreased connectivity in these regions has been linked to memory deficits observed in AD [68]. **Temporal_Pole_Sup_L (ROI 64)**: The superior temporal pole is involved in social and emotional processing. Studies have indicated altered connectivity in this region, which may contribute to the emotional and social cognition deficits seen in AD [69, 70]. **Occipital_Inf_L, Occipital_Mid_L (ROIs 8, 154, 156, 159)**: Occipital regions are less frequently discussed in AD research, but alterations in visual processing areas can affect visuospatial skills. Some studies report changes in connectivity in occipital regions, which may be secondary to higher-order network dysfunctions [71]. While less common, our findings contribute to growing evidence that occipital connectivity might also be disrupted in AD. **Lingual_L (ROI 12)**: The lingual gyrus is involved in visual processing and memory. Altered connectivity in the lingual gyrus has been associated with memory impairments and visual hallucinations in AD [72]. Our results are consistent with those suggesting a role for visual areas in cognitive deficits in AD. **Precentral_R (ROI 225)**: The precentral gyrus, involved in motor control, has shown altered connectivity in AD, which could relate to motor function changes or reflect broader network disruptions [73]. Although motor areas are less frequently emphasized, our results may reflect emerging findings on widespread network disruptions in AD. **Frontal_Mid_Orb_L (ROI 192)**: Middle Frontal Orbital Gyrus region is part of the executive control network. Reduced connectivity here has been linked to deficits in executive function and decision-making in AD [74]. Our findings support previous reports on frontal connectivity changes and their cognitive implications in AD. **Fusiform_L (ROI 5)**: The fusiform gyrus is crucial for facial recognition and processing. Studies have shown altered connectivity in the fusiform gyrus, which might contribute to the visual and recognition deficits in AD [75]. Changes in the fusiform gyrus connectivity are consistent with known cognitive impairments in AD.

Our findings are largely consistent with existing literature on altered functional connectivity in AD, supporting the idea that these regions are involved in the disease's pathology. These results provide additional evidence for the disruption of networks related to memory, executive function, and visual processing in AD. This alignment with previous research underscores the robustness of our results and their contribution to understanding AD's functional connectivity landscape.

The third column of Table 2 shows significant edges/connections in comparison of functional connectivity matrices of three groups of HC, MCI, and AD. The most frequent edge which showed significant differences between groups was the left angular gyrus (Angular_L) to the left middle occipital gyrus (Occipital_Mid_L) connection. The angular gyrus is part of the DMN, which is crucial for cognitive functions such as memory retrieval, attention, and processing of semantic information. As stated above, it is often implicated in cognitive decline associated with AD and MCI. The occipital cortex, including the middle occipital gyrus, is primarily involved in visual processing. However, it also plays a role in integrating visual information with other cognitive processes, which can be disrupted in neurodegenerative conditions. The DMN, which includes the angular gyrus, is consistently found to be disrupted in AD and MCI. Reduced functional connectivity within the DMN, including the connectivity between the angular gyrus and other regions, has been reported in various studies [76]. Specifically, reduced connectivity between the angular gyrus and visual processing regions, like the middle occipital gyrus, may reflect the early cognitive deficits seen in MCI and the progression to AD. This includes impairments in visuospatial processing and memory [77]. Studies have shown that in AD and MCI patients, there is a notable reduction in connectivity between the angular gyrus and regions involved in sensory processing, such as the occipital cortex. This reduction may contribute to the characteristic

symptoms of AD, including memory loss, difficulty with visual-spatial tasks, and overall cognitive decline [76-78]. The altered connectivity we observed could indicate a disruption in how these regions communicate, leading to deficits in integrating visual information with other cognitive processes, which is crucial for tasks like recognizing faces, objects, or navigating environments.

Looking at rows of Table 2, we can investigate the alterations in brain functional connectivity between three groups, at different resolutions. The original connectivity matrix represents the functional connectivity between different brain regions based on the original, non-decomposed rs-fMRI signals. The sparse matrix of significant differences derived from this data indicates which connections between brain regions show statistically significant differences between the groups (AD, MCI, and HC) (Table 3). Each of the five decomposed connectivity matrices represents functional connectivity at different temporal scales or frequency bands, as determined by the DWT (Table 2). The sparse matrices of significant differences for these decomposed levels indicate which connections at specific frequency bands differ significantly between the groups. Level 1 (Highest Frequency/Lowest Scale) captures the most transient, high-frequency interactions in brain activity and Level 5 (Lowest Frequency/Highest Scale) captures more sustained, low-frequency interactions. Following disrupted regions were found at the first level of decomposition: "Angular_L (ROI 99), Temporal_Inf_R (ROI 26), Temporal_Mid_L (ROI 250), Temporal_Pole_Sup_L (64), Occipital_Inf_L (ROIs 8, 154), Occipital_Mid_L (ROIs 156, 159), Lingual_L (ROI 12)". The most disrupted brain regions at the fifth level of decomposition were as follows: Temporal_Mid_R (ROI 147), Frontal_Inf_Orb_R (ROIs 224, 205), Frontal_Inf_Tri_L (ROI 190), and Occipital_Inf_L (ROI 154). The disruptions at the first level of decomposition primarily reflect impairments in rapid, localized brain processes. These regions are more involved in tasks that require quick, dynamic responses, such as visual recognition, language

comprehension, and sensory integration. In contrast, the disruptions at the fifth level of decomposition are related to more sustained, long-term interactions across broader brain networks. These regions support more stable cognitive functions, such as long-term memory, decision-making, and emotional regulation. Both the first and fifth levels show disruptions in occipital regions (e.g., Occipital_Inf_L), indicating that visual processing is affected at both transient and stable levels of connectivity. Similarly, temporal regions are disrupted at both levels, highlighting their role in language and memory processing across different temporal scales. The first level includes the left angular gyrus, superior temporal pole, and lingual gyrus, which are associated with rapid processing and integration of sensory, emotional, and visual information. This suggests that AD and MCI might disrupt the brain's ability to quickly process and respond to environmental stimuli. The fifth level includes regions like the inferior frontal gyrus (orbital and triangular parts), which are associated with stable, long-range cognitive control, decision-making, and language production. These disruptions reflect more profound and sustained impairments in higher-order cognitive functions.

At the second phase of our experiments, we derived graph theoretical measures from brain complex networks to accurately discriminate between patients with AD, patients with MCI, and control subjects. Graph theoretical based measures employed to quantify alteration in functional connectivity of brain networks, in original and decomposed forms, due to the AD and MCI. Various measures of graph segregation, integration, and resilience were extracted and fed to the classifier as discriminative features. Filter and wrapper feature selection methods were employed to select the most efficient features. We selected a set of optimal features. To this end, we used the Fisher algorithm as a filter at the first stage of feature selection. We used FSFS in a wrapper fashion at the second stage of feature selection.

Selecting an appropriate learning algorithm (classifier) is critical. Various classifiers have been used in bioinformatics literature, including k -nearest neighbor, naïve Bayes, Fisher linear, linear discriminant, quadratic classifier, decision tree, and SVM with linear, polynomial and RBF kernels. SVM with RBF kernel and naïve Bayes classifier outperformed other classifiers in terms of accuracy, sensitivity, specificity, and positive predictivity, in our previous study [11]. Detailed results in Tables 4-7 provide accuracies of employing different wavelet types at different levels of decomposition for classification of three groups of HC, MCI, and AD using SVM and naïve Bayes classifier. The classification using graph measures of brain networks obtained from original rs-fMRI signals, were 80% for SVM and 95.7895% for Bayes classifier. There are improvements in the accuracies when using DWT decomposed rs-fMRI signals. Figures 8 and 9 illustrate the distribution plot of data within Tables 4-7 and red lines are classification accuracies using original rs-fMRI signals without wavelet decomposition. Overall, the naïve Bayes classifier provided much better performance rather than the SVM. Figure 10 plots their performances over all wavelet types at different levels of decomposition. From Tables 4-7 it can be seen that in most cases, the level 5 decomposition resulted in the best classification accuracy among other levels of decomposition for each type of mother wavelets. In 14 wavelet types, level 5 of decomposition; in 5 wavelet types, level 4 of decomposition; and eventually in one wavelet type, the level 3 of decomposition; resulted in the best classification accuracy, among other levels of decomposition (Tables 4-7). These results suggest that the low-frequency components are particularly informative for distinguishing between HC, MCI, and AD. This aligns with the idea that low-frequency brain signals are associated with stable, long-range interactions in the brain, which are more likely to be disrupted in neurodegenerative diseases like AD. The first level of decomposition, capturing high-frequency components, shows variable classification accuracies depending on the wavelet type used. For

example, while Naïve Bayes classifier achieved 95.789% accuracy with db1 wavelets, the accuracies generally decreased across other wavelets, especially with SVM. High-frequency components reflect more transient, localized brain processes. The less consistent performance at this level suggests that these features might not be as robust or universally discriminative for AD, MCI, and HC differentiation.

5- Conclusions

We applied the graph theoretical approach and the pattern recognition method on the resting state fMRI data to classify three groups: normal controls, patients with AD, and patients with MCI. The proposed method identified a specific sets of brain regions and functional connections that are informative to distinguish three groups (i.e. Controls, MCI, and AD). Our findings reveal that certain brain networks, particularly those related to the default mode network (DMN) and visual processing regions, are significantly disrupted in AD and MCI patients. Most of these regions and connections were consistent in different frequency bands, as illustrated in our DWT-based decomposed graphs at various levels of decomposition. There were also some differences between frequency bands, that approve the dynamic nature of brain functionality and rs-fMRI oscillations. The use of DWT-decomposed graphs provided enhanced classification accuracy, especially at higher levels of decomposition, indicating that low-frequency brain signals, which represent more stable and long-range interactions, are particularly informative for distinguishing between AD, MCI, and healthy subjects. This multi-scale approach not only improves the classification performance but also offers deeper insights into the frequency-specific alterations in brain connectivity associated with neurodegenerative diseases. These results

demonstrate the potential of combining advanced signal processing techniques with graph theoretical measures to better understand and diagnose AD and MCI.

Ethical approval: All procedures performed in studies involving human participants were in accordance with the ethical standards of the institutional and/or national research committee and with the 1964 Helsinki declaration and its later amendments or comparable ethical standards.

Informed consent: Informed consent was obtained from all individual participants included in the study.

Acknowledgments: Data used in this paper were obtained from the Alzheimer's Disease Neuroimaging Initiative (ADNI) database (<http://ADNI.loni.usc.edu>). The investigators within the ADNI, who can be found at <http://ADNI.loni.usc.edu/study-design/ongoing-investigations>, contributed to the design and implementation of ADNI and/or provided data but did not participate in analysis or writing of this article. Data collection and sharing for this project was funded by the Alzheimer's Disease Neuroimaging Initiative (ADNI) (National Institutes of Health Grant U01 AG024904). ADNI is funded by the National Institute on Aging, the National Institute of Biomedical Imaging and Bioengineering, and through generous contributions from the following: AbbVie, Alzheimer's Association; Alzheimer's Drug Discovery Foundation; Araclon Biotech; BioClinica, Inc.; Biogen; Bristol-Myers Squibb Company; CereSpir, Inc.; Eisai Inc.; Elan Pharmaceuticals, Inc.; Eli Lilly and Company; EuroImmun; F. Hoffmann-La Roche Ltd and its

affiliated company Genentech, Inc.; Fujirebio; GE Healthcare; IXICO Ltd.; Janssen Alzheimer Immunotherapy Research & Development, LLC.; Johnson & Johnson Pharmaceutical Research & Development LLC.; Lumosity; Lundbeck; Merck & Co., Inc.; Meso Scale Diagnostics, LLC.; NeuroRx Research; Neurotrack Technologies; Novartis Pharmaceuticals Corporation; Pfizer Inc.; Piramal Imaging; Servier; Takeda Pharmaceutical Company; and Transition Therapeutics. The Canadian Institutes of Health Research is providing funds to support ADNI clinical sites in Canada. Private sector contributions are facilitated by the Foundation for the National Institutes of Health (www.fnih.org). The grantee organization is the Northern California Institute for Research and Education, and the study is coordinated by the Alzheimer's Disease Cooperative Study at the University of California, San Diego. ADNI data are disseminated by the Laboratory for Neuro Imaging at the University of Southern California.

Financial Disclosures: The authors report no biomedical financial interests or potential conflicts of interest.

References

- [1] R.C. Petersen, G.E. Smith, S.C. Waring, R.J. Ivnik, E.G. Tangalos, E. Kokmen, Mild cognitive impairment: Clinical characterization and outcome, *Archives of Neurology*, 56 (1999) 303-308.
- [2] N.S. Ryan, M.N. Rossor, Defining and describing the pre-dementia stages of familial Alzheimer's disease, *Alzheimers Res Ther*, 3 (2011) 29.

- [3] C.E. Conti Filho, L.B. Loss, C. Marcolongo-Pereira, J.V. Rossoni Junior, R.M. Barcelos, O. Chiarelli-Neto, B.S.d. Silva, R. Passamani Ambrosio, F.C.d.A.Q. Castro, S.F. Teixeira, N.J. Mezzomo, Advances in Alzheimer's disease's pharmacological treatment, *Frontiers in Pharmacology*, 14 (2023).
- [4] Y. Shigihara, H. Hoshi, K. Shinada, T. Okada, H. Kamada, Non-pharmacological treatment changes brain activity in patients with dementia, *Scientific Reports*, 10 (2020) 6744.
- [5] M.S.E. Sendi, E. Zendeihrouh, Z. Fu, J. Liu, Y. Du, E. Mormino, D.H. Salat, V.D. Calhoun, R.L. Miller, Disrupted Dynamic Functional Network Connectivity Among Cognitive Control Networks in the Progression of Alzheimer's Disease, *Brain Connect*, 13 (2023) 334-343.
- [6] N.L. Komarova, C.J. Thalhauser, High degree of heterogeneity in Alzheimer's disease progression patterns, *PLoS Comput Biol*, 7 (2011) e1002251.
- [7] M.C. Litwińczuk, N. Trujillo-Barreto, N. Muhlert, L. Cloutman, A. Woollams, Relating cognition to both brain structure and function: A systematic review of methods, *Brain Connectivity*, 13 (2023) 120-132.
- [8] C. Yen, C.-L. Lin, M.-C. Chiang, Exploring the Frontiers of Neuroimaging: A Review of Recent Advances in Understanding Brain Functioning and Disorders, *Life*, 13 (2023) 1472.
- [9] E.E. Tulay, B. Metin, N. Tarhan, M.K. Arıkan, Multimodal Neuroimaging: Basic Concepts and Classification of Neuropsychiatric Diseases, *Clinical EEG and Neuroscience*, 50 (2018) 20-33.
- [10] S.H. Hojjati, A. Ebrahimzadeh, A. Babajani-Feremi, Identification of the Early Stage of Alzheimer's Disease Using Structural MRI and Resting-State fMRI, *Frontiers in Neurology*, 10 (2019).
- [11] A. Khazaei, A. Ebrahimzadeh, A. Babajani-Feremi, Classification of patients with MCI and AD from healthy controls using directed graph measures of resting-state fMRI, *Behav Brain Res*, 322 (2017) 339-350.
- [12] M.S.E. Sendi, E. Zendeihrouh, C.A. Ellis, Z. Fu, J. Chen, R.L. Miller, E.C. Mormino, D.H. Salat, V.D. Calhoun, The link between static and dynamic brain functional network connectivity and genetic risk of Alzheimer's disease, *NeuroImage: Clinical*, 37 (2023) 103363.
- [13] S. Shakil, C.-H. Lee, S.D. Keilholz, Evaluation of sliding window correlation performance for characterizing dynamic functional connectivity and brain states, *NeuroImage*, 133 (2016) 111-128.
- [14] X.-Y. Wang, C. Li, R. Zhang, L. Wang, J.-L. Tan, H. Wang, Intelligent Extraction of Salient Feature From Electroencephalogram Using Redundant Discrete Wavelet Transform, *Frontiers in Neuroscience*, 16 (2022).
- [15] L. Mohammadzadeh, H. Latifi, S. Khaksar, M.-S. Feiz, F. Motamedi, A. Asadollahi, M. Ezzatpour, Measuring the Frequency-Specific Functional Connectivity Using Wavelet Coherence Analysis in Stroke Rats Based on Intrinsic Signals, *Scientific Reports*, 10 (2020) 9429.
- [16] R.X. Smith, K. Jann, M. Dapretto, D.J.J. Wang, Imbalance of Functional Connectivity and Temporal Entropy in Resting-State Networks in Autism Spectrum Disorder: A Machine Learning Approach, *Front Neurosci*, 12 (2018) 869.

- [17] A. Bernas, A.P. Aldenkamp, S. Zinger, Wavelet coherence-based classifier: A resting-state functional MRI study on neurodynamics in adolescents with high-functioning autism, *Comput Methods Programs Biomed*, 154 (2018) 143-151.
- [18] M.I. Al-Hiyali, N. Yahya, I. Faye, A.F. Hussein, Identification of Autism Subtypes Based on Wavelet Coherence of BOLD fMRI Signals Using Convolutional Neural Network, *Sensors (Basel)*, 21 (2021).
- [19] R. Cîrstian, J. Pilmeyer, A. Bernas, J.F.A. Jansen, M. Breeuwer, A.P. Aldenkamp, S. Zinger, Objective biomarkers of depression: A study of Granger causality and wavelet coherence in resting-state fMRI, *J Neuroimaging*, 33 (2023) 404-414.
- [20] M. Zhou, B.D. Boyd, W.D. Taylor, H. Kang, Double-wavelet transform for multi-subject resting state functional magnetic resonance imaging data, *Stat Med*, 40 (2021) 6762-6776.
- [21] F.F. Luo, J.B. Wang, L.X. Yuan, Z.W. Zhou, H. Xu, S.H. Ma, Y.F. Zang, M. Zhang, Higher Sensitivity and Reproducibility of Wavelet-Based Amplitude of Resting-State fMRI, *Front Neurosci*, 14 (2020) 224.
- [22] D. Cordes, M.F. Kaleem, Z. Yang, X. Zhuang, T. Curran, K.R. Sreenivasan, V.R. Mishra, R. Nandy, R.R. Walsh, Energy-Period Profiles of Brain Networks in Group fMRI Resting-State Data: A Comparison of Empirical Mode Decomposition With the Short-Time Fourier Transform and the Discrete Wavelet Transform, *Front Neurosci*, 15 (2021) 663403.
- [23] J. Wang, X. Zuo, Z. Dai, M. Xia, Z. Zhao, X. Zhao, J. Jia, Y. Han, Y. He, Disrupted Functional Brain Connectome in Individuals at Risk for Alzheimer's Disease, *Biological Psychiatry*, 73 (2013) 472-481.
- [24] A. Sadiq, N. Yahya, T.B. Tang, H. Hashim, I. Naseem, Wavelet-Based Fractal Analysis of rs-fMRI for Classification of Alzheimer's Disease, *Sensors (Basel)*, 22 (2022).
- [25] Y. Gao, N. Lewis, V.D. Calhoun, R.L. Miller, Interpretable LSTM model reveals transiently-realized patterns of dynamic brain connectivity that predict patient deterioration or recovery from very mild cognitive impairment, *Comput Biol Med*, 161 (2023) 107005.
- [26] E. Bullmore, O. Sporns, Complex brain networks: graph theoretical analysis of structural and functional systems, *Nat Rev Neurosci*, 10 (2009) 186-198.
- [27] B. Jie, D. Zhang, C.Y. Wee, D. Shen, Topological graph kernel on multiple thresholded functional connectivity networks for mild cognitive impairment classification, *Human brain mapping*, 35 (2014) 2876-2897.
- [28] A. Khazaei, A. Ebrahimzadeh, A. Babajani-Feremi, Identifying patients with Alzheimer's disease using resting-state fMRI and graph theory, *Clinical Neurophysiology*, 126 (2015) 2132-2141.
- [29] A. Khazaei, A. Ebrahimzadeh, A. Babajani-Feremi, Application of advanced machine learning methods on resting-state fMRI network for identification of mild cognitive impairment and Alzheimer's disease, *Brain Imaging and Behavior*, 10 (2016) 799-817.
- [30] I.O. Korolev, L.L. Symonds, A.C. Bozoki, I. Alzheimer's Disease Neuroimaging, Predicting Progression from Mild Cognitive Impairment to Alzheimer's Dementia Using Clinical, MRI, and Plasma Biomarkers via Probabilistic Pattern Classification, *PLOS ONE*, 11 (2016) e0138866.

- [31] C.R. Jack, Jr., M.A. Bernstein, N.C. Fox, P. Thompson, G. Alexander, D. Harvey, B. Borowski, P.J. Britson, L.W. J. C. Ward, A.M. Dale, J.P. Felmlee, J.L. Gunter, D.L. Hill, R. Killiany, N. Schuff, S. Fox-Bosetti, C. Lin, C. Studholme, C.S. DeCarli, G. Krueger, H.A. Ward, G.J. Metzger, K.T. Scott, R. Mallozzi, D. Blezek, J. Levy, J.P. Debbins, A.S. Fleisher, M. Albert, R. Green, G. Bartzokis, G. Glover, J. Mugler, M.W. Weiner, The Alzheimer's Disease Neuroimaging Initiative (ADNI): MRI methods, *J Magn Reson Imaging*, 27 (2008) 685-691.
- [32] K.J. Friston, C.D. Frith, R.S. Frackowiak, R. Turner, Characterizing dynamic brain responses with fMRI: a multivariate approach, *Neuroimage*, 2 (1995) 166-172.
- [33] M.D. Fox, A.Z. Snyder, J.L. Vincent, M. Corbetta, D.C. Van Essen, M.E. Raichle, The human brain is intrinsically organized into dynamic, anticorrelated functional networks, *Proceedings of the National Academy of Sciences of the United States of America*, 102 (2005) 9673-9678.
- [34] P. Fransson, Spontaneous low-frequency BOLD signal fluctuations: An fMRI investigation of the resting-state default mode of brain function hypothesis, *Human brain mapping*, 26 (2005) 15-29.
- [35] M.D. Greicius, B. Krasnow, A.L. Reiss, V. Menon, Functional connectivity in the resting brain: a network analysis of the default mode hypothesis, *Proceedings of the National Academy of Sciences*, 100 (2003) 253-258.
- [36] A. Kelly, L.Q. Uddin, B.B. Biswal, F.X. Castellanos, M.P. Milham, Competition between functional brain networks mediates behavioral variability, *Neuroimage*, 39 (2008) 527-537.
- [37] Y. Chao-Gan, Z. Yu-Feng, DPARSF: A MATLAB Toolbox for "Pipeline" Data Analysis of Resting-State fMRI, *Front Syst Neurosci*, 4 (2010) 13.
- [38] J.D. Power, A.L. Cohen, S.M. Nelson, G.S. Wig, K.A. Barnes, J.A. Church, A.C. Vogel, T.O. Laumann, F.M. Miezin, B.L. Schlaggar, S.E. Petersen, Functional network organization of the human brain, *Neuron*, 72 (2011) 665-678.
- [39] M.P. van den Heuvel, O. Sporns, Network hubs in the human brain, *Trends in cognitive sciences*, 17 (2013) 683-696.
- [40] S.I. Dimitriadis, N.A. Laskaris, V. Tsirka, M. Vourkas, S. Micheloyannis, S. Fotopoulos, Tracking brain dynamics via time-dependent network analysis, *Journal of Neuroscience Methods*, 193 (2010) 145-155.
- [41] M. Rubinov, O. Sporns, Complex network measures of brain connectivity: uses and interpretations, *Neuroimage*, 52 (2010) 1059-1069.
- [42] D.J. Watts, S.H. Strogatz, Collective dynamics of 'small-world' networks, *nature*, 393 (1998) 440-442.
- [43] V. Latora, M. Marchiori, Efficient behavior of small-world networks, *Physical review letters*, 87 (2001) 198701.
- [44] R. Guimera, M. Sales-Pardo, L.A. Amaral, Classes of complex networks defined by role-to-role connectivity profiles, *Nature physics*, 3 (2007) 63-69.
- [45] M. Rubinov, O. Sporns, Weight-conserving characterization of complex functional brain networks, *Neuroimage*, 56 (2011) 2068-2079.

- [46] U. Brandes, A faster algorithm for betweenness centrality*, *Journal of Mathematical Sociology*, 25 (2001) 163-177.
- [47] P. Hagmann, L. Cammoun, X. Gigandet, R. Meuli, C.J. Honey, V.J. Wedeen, O. Sporns, Mapping the structural core of human cerebral cortex, *PLoS biology*, 6 (2008) e159.
- [48] E. Estrada, D.J. Higham, Network properties revealed through matrix functions, *SIAM review*, 52 (2010) 696-714.
- [49] M.E.J. Newman, mathematics of networks, in: S.N. Durlauf, L.E. Blume (Eds.) *The New Palgrave Dictionary of Economics*, Palgrave Macmillan, Basingstoke, 2008.
- [50] P. Boldi, M. Santini, S. Vigna, PageRank: functional dependencies, *ACM Transactions on Information Systems (TOIS)*, 27 (2009) 19.
- [51] J.G. Foster, D.V. Foster, P. Grassberger, M. Paczuski, Edge direction and the structure of networks, *Proceedings of the National Academy of Sciences*, 107 (2010) 10815-10820.
- [52] M.D. Humphries, K. Gurney, Network ‘small-world-ness’: a quantitative method for determining canonical network equivalence, *PloS one*, 3 (2008) e0002051.
- [53] A. Zalesky, A. Fornito, E.T. Bullmore, Network-based statistic: identifying differences in brain networks, *Neuroimage*, 53 (2010) 1197-1207.
- [54] C.R. Genovese, N.A. Lazar, T. Nichols, Thresholding of Statistical Maps in Functional Neuroimaging Using the False Discovery Rate, *NeuroImage*, 15 (2002) 870-878.
- [55] R.O. Duda, P.E. Hart, D.G. Stork, *Pattern classification*, John Wiley & Sons, 2012.
- [56] V. Vapnik, *Statistical learning theory*. 1998, in, Wiley, New York, 1998.
- [57] T.M. Mitchell, R. Hutchinson, R.S. Niculescu, F. Pereira, X. Wang, M. Just, S. Newman, Learning to Decode Cognitive States from Brain Images, *Machine Learning*, 57 (2004) 145-175.
- [58] J.L. Hellerstein, T. Jayram, I. Rish, Recognizing end-user transactions in performance management, IBM Thomas J. Watson Research Division, 2000.
- [59] P. Domingos, M. Pazzani, On the optimality of the simple Bayesian classifier under zero-one loss, *Machine learning*, 29 (1997) 103-130.
- [60] I. Rish, J. Hellerstein, J. Thathachar, An analysis of data characteristics that affect naive Bayes performance, IBM TJ Watson Research Center, 30 (2001).
- [61] E.J. Sanz-Arigita, M.M. Schoonheim, J.S. Damoiseaux, S.A.R.B. Rombouts, E. Maris, F. Barkhof, P. Scheltens, C.J. Stam, Loss of ‘Small-World’ Networks in Alzheimer's Disease: Graph Analysis of fMRI Resting-State Functional Connectivity, *PLoS ONE*, 5 (2010) e13788.
- [62] F. Bai, W. Liao, D.R. Watson, Y. Shi, Y. Wang, C. Yue, Y. Teng, D. Wu, Y. Yuan, J. Jia, Abnormal whole-brain functional connection in amnesic mild cognitive impairment patients, *Behavioural brain research*, 216 (2011) 666-672.

- [63] Z. Wang, X. Jia, P. Liang, Z. Qi, Y. Yang, W. Zhou, K. Li, Changes in thalamus connectivity in mild cognitive impairment: Evidence from resting state fMRI, *European journal of radiology*, 81 (2012) 277-285.
- [64] C.-Y. Wee, P.-T. Yap, D. Zhang, K. Denny, J.N. Browndyke, G.G. Potter, K.A. Welsh-Bohmer, L. Wang, D. Shen, Identification of MCI individuals using structural and functional connectivity networks, *Neuroimage*, 59 (2012) 2045-2056.
- [65] R.L. Buckner, J.R. Andrews-Hanna, D.L. Schacter, The brain's default network: anatomy, function, and relevance to disease, *Annals of the new York Academy of Sciences*, 1124 (2008) 1-38.
- [66] C. Sorg, V. Riedl, M. Mühlau, V.D. Calhoun, T. Eichele, L. Läer, A. Drzezga, H. Förstl, A. Kurz, C. Zimmer, Selective changes of resting-state networks in individuals at risk for Alzheimer's disease, *Proceedings of the National Academy of Sciences*, 104 (2007) 18760-18765.
- [67] S.A. Murai, T. Mano, J.N. Sanes, T. Watanabe, Atypical intrinsic neural timescale in the left angular gyrus in Alzheimer's disease, *Brain Communications*, 6 (2024).
- [68] L. Wang, Y. Zang, Y. He, M. Liang, X. Zhang, L. Tian, T. Wu, T. Jiang, K. Li, Changes in hippocampal connectivity in the early stages of Alzheimer's disease: evidence from resting state fMRI, *Neuroimage*, 31 (2006) 496-504.
- [69] W.W. Seeley, R.K. Crawford, J. Zhou, B.L. Miller, M.D. Greicius, Neurodegenerative diseases target large-scale human brain networks, *Neuron*, 62 (2009) 42-52.
- [70] S. Schwab, S. Afyouni, Y. Chen, Z. Han, Q. Guo, T. Dierks, L.O. Wahlund, M. Grieder, Functional Connectivity Alterations of the Temporal Lobe and Hippocampus in Semantic Dementia and Alzheimer's Disease, *J Alzheimers Dis*, 76 (2020) 1461-1475.
- [71] S. Cai, T. Chong, Y. Peng, W. Shen, J. Li, K.M. von Deneen, L. Huang, Altered functional brain networks in amnesic mild cognitive impairment: a resting-state fMRI study, *Brain Imaging Behav*, 11 (2017) 619-631.
- [72] D. Zhen, W. Xia, Z.Q. Yi, P.W. Zhao, J.G. Zhong, H.C. Shi, H.L. Li, Z.Y. Dai, P.L. Pan, Alterations of brain local functional connectivity in amnesic mild cognitive impairment, *Transl Neurodegener*, 7 (2018) 26.
- [73] X.-a. Bi, Q. Jiang, Q. Sun, Q. Shu, Y. Liu, Analysis of Alzheimer's Disease Based on the Random Neural Network Cluster in fMRI, *Frontiers in Neuroinformatics*, 12 (2018).
- [74] M. Dai, Z. Guo, J. Chen, H. Liu, J. Li, M. Zhu, J. Liu, F. Wei, L. Wang, X. Liu, Altered functional connectivity of the locus coeruleus in Alzheimer's disease patients with depression symptoms, *Experimental Gerontology*, 179 (2023) 112252.
- [75] J. Huang, P. Beach, A. Bozoki, D.C. Zhu, Alzheimer's Disease Progressively Reduces Visual Functional Network Connectivity, *J Alzheimers Dis Rep*, 5 (2021) 549-562.
- [76] B. Ibrahim, S. Suppiah, N. Ibrahim, M. Mohamad, H.A. Hassan, N.S. Nasser, M.I. Saripan, Diagnostic power of resting-state fMRI for detection of network connectivity in Alzheimer's disease and mild cognitive impairment: A systematic review, *Human brain mapping*, 42 (2021) 2941-2968.

[77] S. Huang, S. Wang, Z. Che, H. Ge, Z. Yan, J. Fan, X. Lu, L. Liu, W. Liu, Y. Zhong, C. Zou, J. Rao, J. Chen, Brain-wide functional connectivity alterations and their cognitive correlates in subjective cognitive decline, *Frontiers in Neuroscience*, 18 (2024).

[78] F. Agosta, M. Pievani, C. Geroldi, M. Copetti, G.B. Frisoni, M. Filippi, Resting state fMRI in Alzheimer's disease: beyond the default mode network, *Neurobiology of aging*, 33 (2012) 1564-1578.

Table 1: Demographic of control subjects, patients with MCI, and patients with AD. MMSE: Mini-Mental State Examination; CDR: Clinical Dementia Rating.

	Healthy Control	Patients with MCI	Patients with AD
Number	45	89	34
Male/Female	19/26	43/46	16/18
Age	75.9±6.79	71.77±7.78	72.54±7.02
MMSE score	28.95±1.56	27.56±2.2	21.24±3.37
CDR score	0.07±0.21	0.49±0.17	0.92±0.31

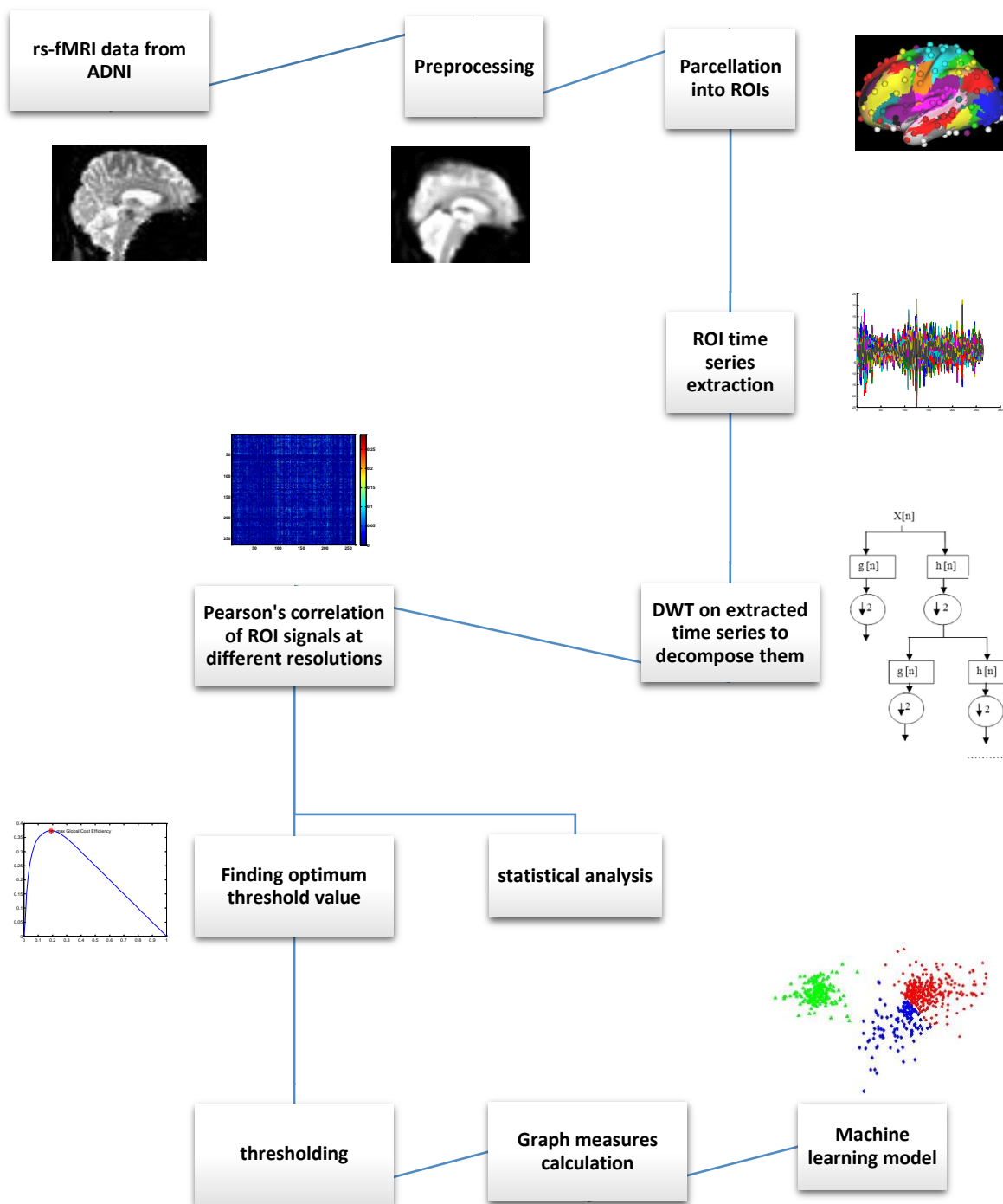


Figure 1: The detailed workflow for the proposed method. The workflow begins with the acquisition of rs-fMRI data from the ADNI database. The steps are as follows: preprocessing the

fMRI data, parcellating the brain into ROIs, extracting time series from these ROIs, and applying DWT to decompose the time series. Subsequent steps involve calculating Pearson's correlation coefficients for ROI signals at various resolutions, determining the optimal threshold value for graph construction, and computing graph measures. The final stages include inputting the computed measures into a machine learning model and statistical analysis.

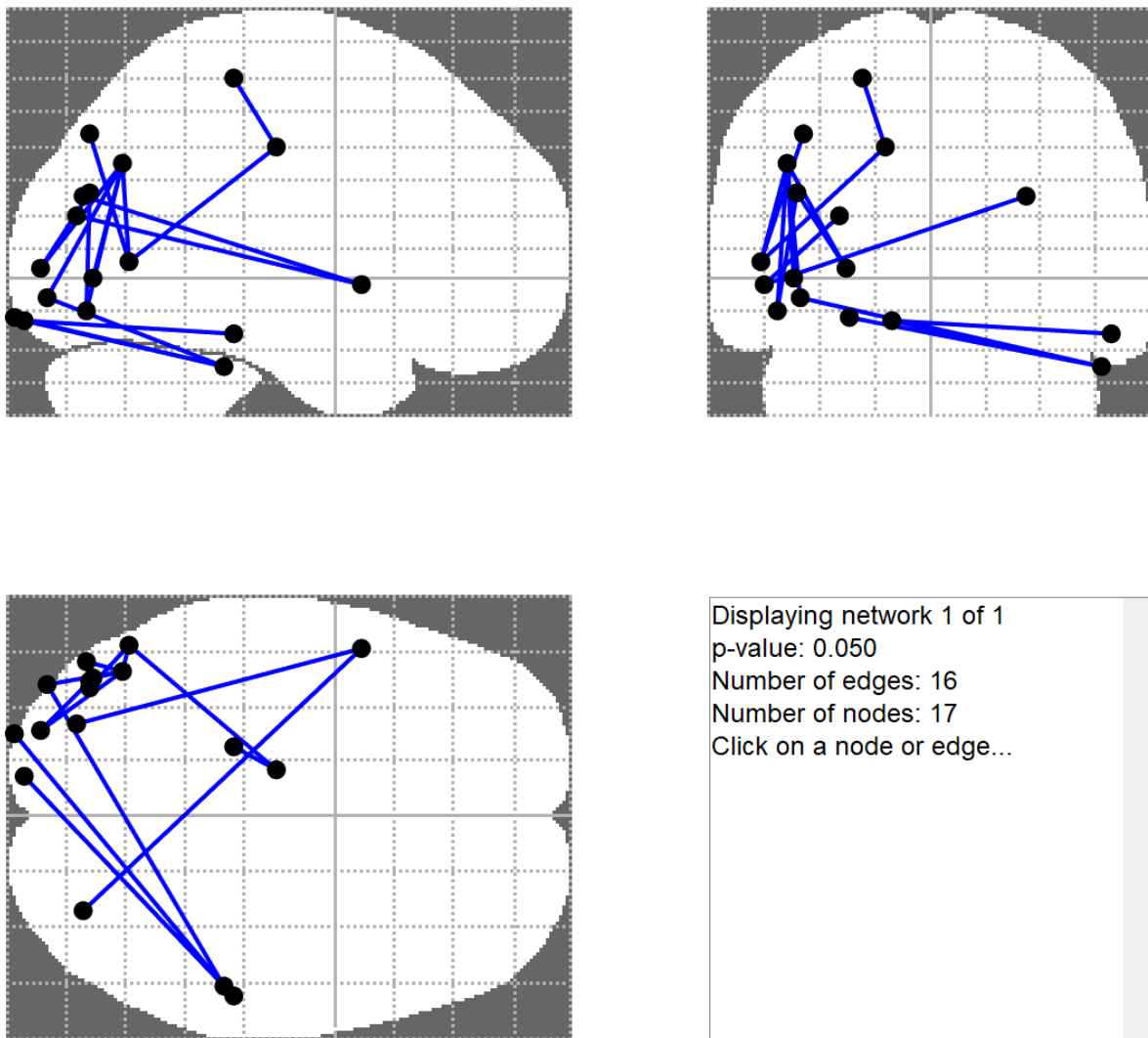


Figure 2: Connections with significant differences between HC, MCI, and AD groups. Original rs-fMRI signals were used to construct raw connectivity matrices for FDR analysis. The statistical analysis using the False Discovery Rate (FDR) method implemented in network-based statistics (NBS) toolbox

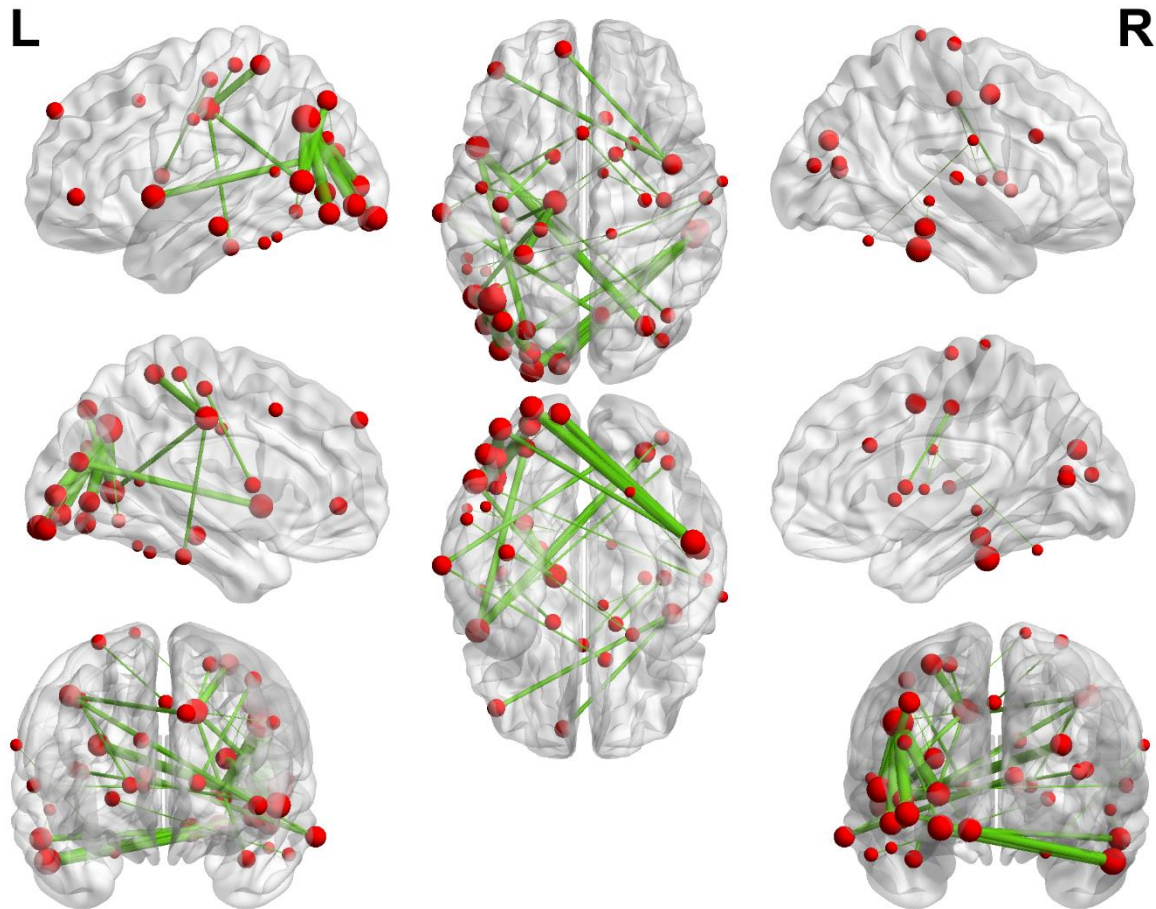


Figure 3: Nodes and edges with significant differences between three groups of HC, MCI, and AD. Approximation coefficients of level 1 decomposition of rs-fMRI signals were used to construct raw connectivity matrices. The results of FDR analysis for 20 different wavelet types (Tables 3-6) were accumulated. The greater the size of nodes and edges, the more frequent node and edge. The size of nodes is the strength of node in the accumulated matrix. The size of each edge is the weight of corresponding connection in the accumulated matrix (the number of appearances of that edge in FDR analysis on raw connectivity matrices of level1 decomposition for 20 different wavelet types). Plots of this figure were created using the BrainNet Viewer software package (<http://nitrc.org/projects/bnv/>).

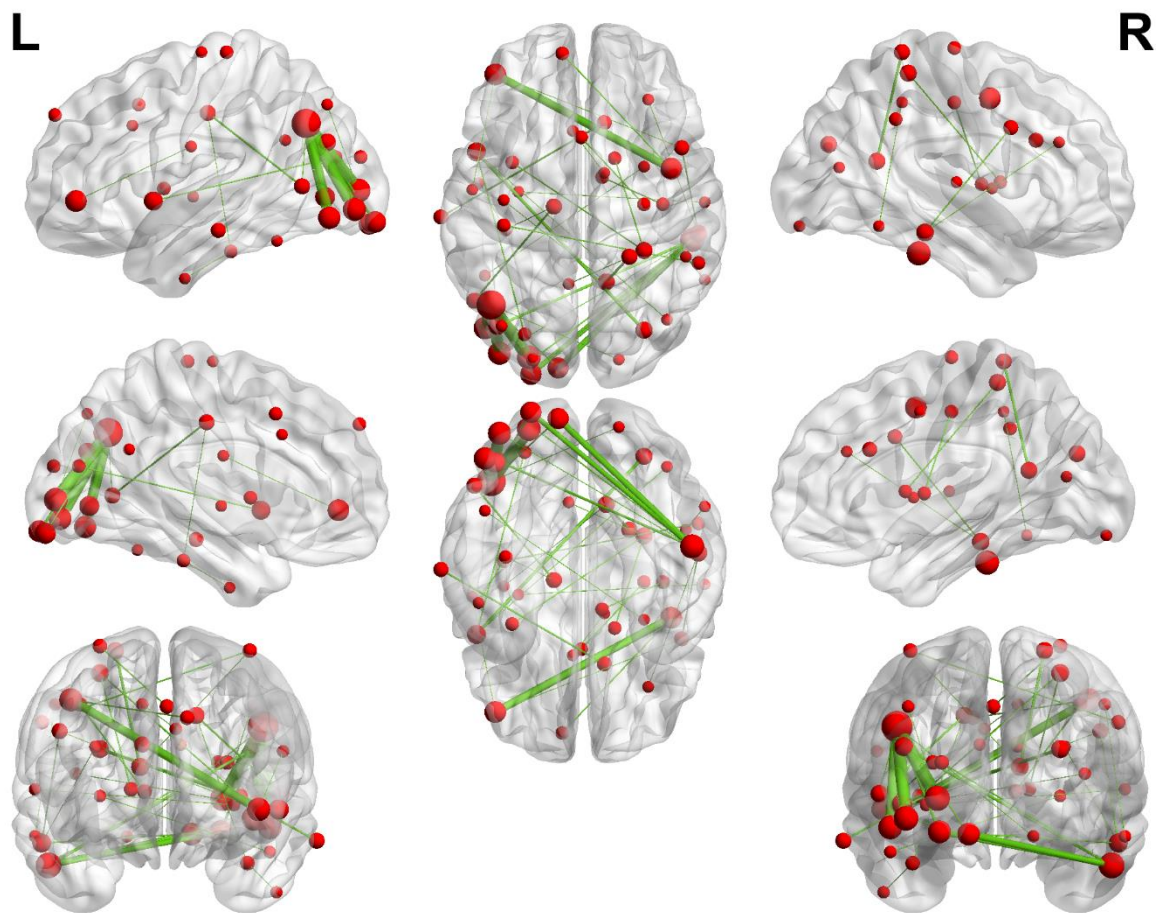


Figure 4: Nodes and edges with significant differences between three groups of HC, MCI, and AD. Approximation coefficients of level 2 decomposition of rs-fMRI signals were used to construct raw connectivity matrices. The results of FDR analysis for 20 different wavelet types (Tables 3-6) were accumulated. The greater the size of nodes and edges, the more frequent node and edge. The size of nodes is the strength of node in the accumulated matrix. The size of each edge is the weight of corresponding connection in the accumulated matrix (the number of appearances of that edge in FDR analysis on raw connectivity matrices of level 2 decomposition for 20 different wavelet types). Plots of this figure were created using the BrainNet Viewer software package (<http://nitrc.org/projects/bnv/>).

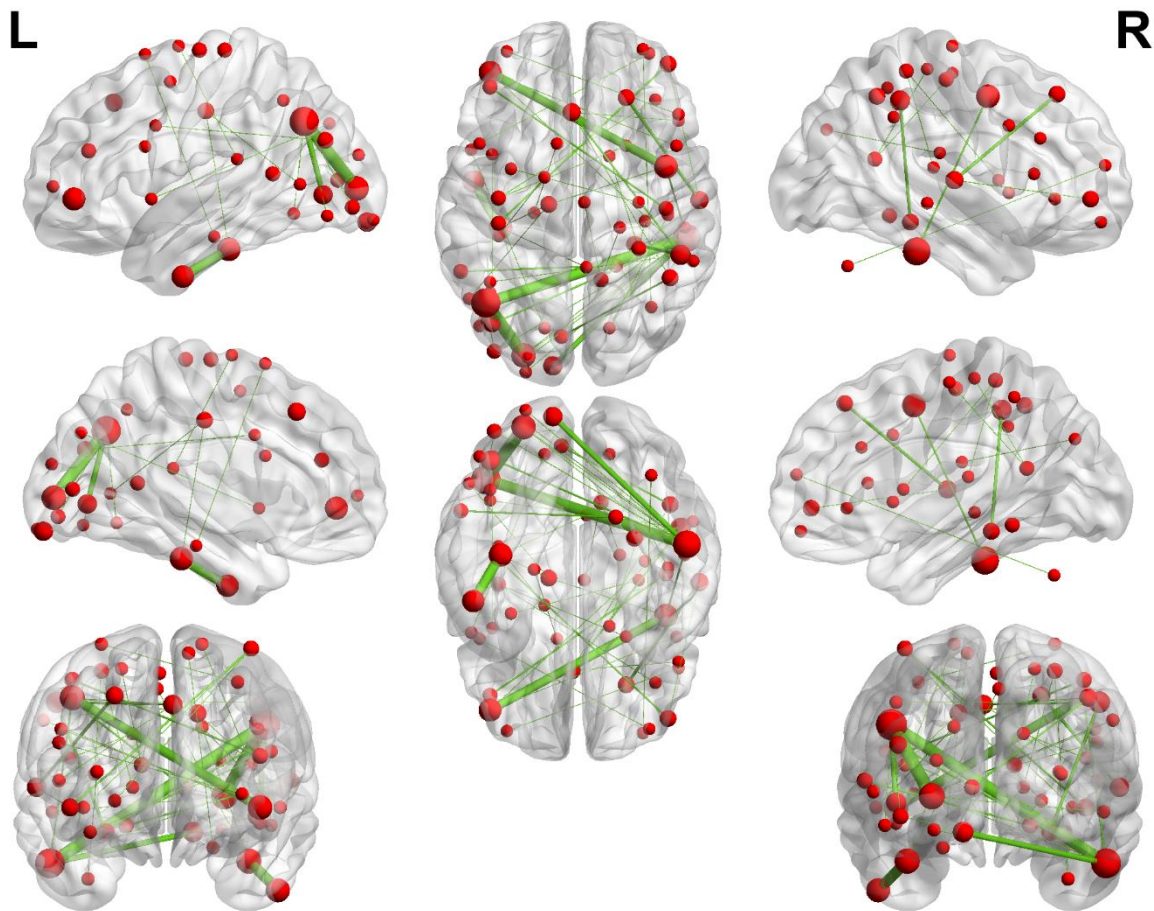


Figure 5: Nodes and edges with significant differences between three groups of HC, MCI, and AD. Approximation coefficients of level 3 decomposition of rs-fMRI signals were used to construct raw connectivity matrices. The results of FDR analysis for 20 different wavelet types (Tables 3-6) were accumulated. The greater the size of nodes and edges, the more frequent node and edge. The size of nodes is the strength of node in the accumulated matrix. The size of each edge is the weight of corresponding connection in the accumulated matrix (the number of appearances of that edge in FDR analysis on raw connectivity matrices of level 3 decomposition for 20 different wavelet types). Plots of this figure were created using the BrainNet Viewer software package (<http://nitrc.org/projects/bnv/>).

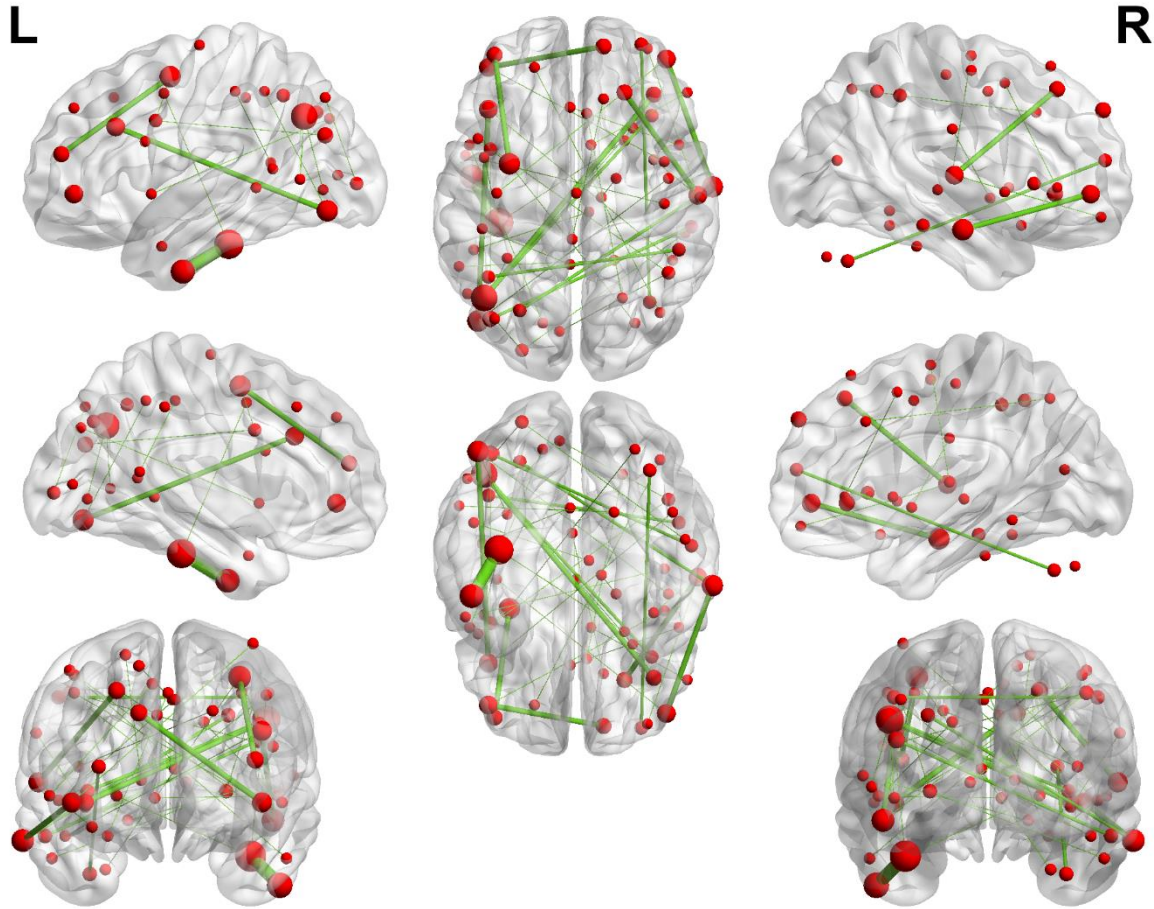


Figure 6: Nodes and edges with significant differences between three groups of HC, MCI, and AD. Approximation coefficients of level 4 decomposition of rs-fMRI signals were used to construct raw connectivity matrices. The results of FDR analysis for 20 different wavelet types (Tables 3-6) were accumulated. The greater the size of nodes and edges, the more frequent node and edge. The size of nodes is the strength of node in the accumulated matrix. The size of each edge is the weight of corresponding connection in the accumulated matrix (the number of appearances of that edge in FDR analysis on raw connectivity matrices of level 4 decomposition for 20 different wavelet types). Plots of this figure were created using the BrainNet Viewer software package (<http://nitrc.org/projects/bnv/>).

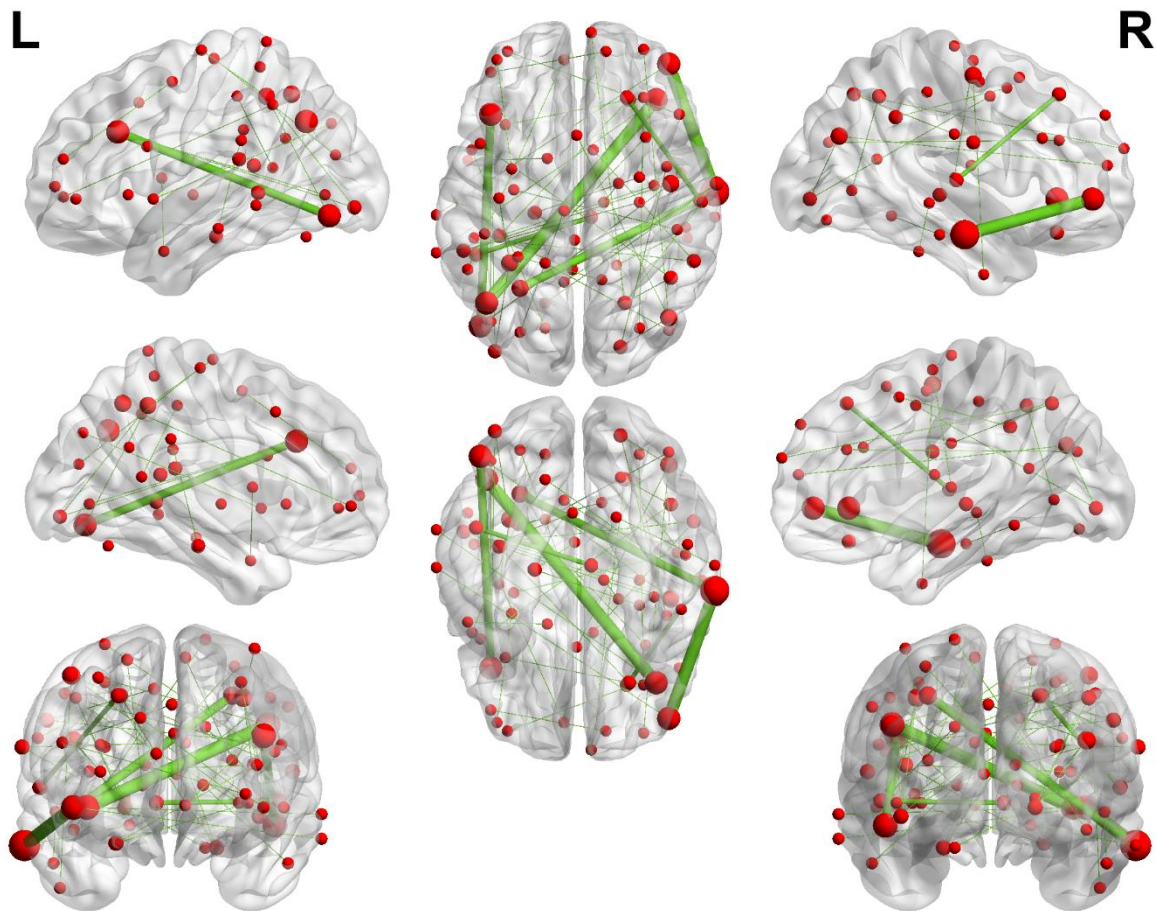


Figure 7: Nodes and edges with significant differences between three groups of HC, MCI, and AD. Approximation coefficients of level 5 decomposition of rs-fMRI signals were used to construct raw connectivity matrices. The results of FDR analysis for 20 different wavelet types (Tables 3-6) were accumulated. The greater the size of nodes and edges, the more frequent node and edge. The size of nodes is the strength of node in the accumulated matrix. The size of each edge is the weight of corresponding connection in the accumulated matrix (the number of appearances of that edge in FDR analysis on raw connectivity matrices of level 5 decomposition for 20 different wavelet types). Plots of this figure were created using the BrainNet Viewer software package (<http://nitrc.org/projects/bnv/>).

Table 2: Significant nodes and connections (edges) in the aggregated FDR matrix. The aggregated FDR matrix was resulted by aggregating 20 sparse matrices of significant connections. Each matrix of significant connection was obtained by applying FDR analysis on connectivity matrices of three groups of HC, MCI, and AD. These connectivity matrices were resulted by correlating decomposed rs-fMRI signals using 20 different wavelet types at specified level of decomposition.

level of decomposition of rs-fMRI signals. The approximate coefficients of decomposed signals were then correlated to construct connectivity matrices for three groups of HC, MCI, and AD	Most frequent significant nodes across 20 different wavelet types.		Most frequent significant connections (edges) across 20 different wavelet types.	
	ROI No. (from 264 putative functional area atlas)	Strength of nodes in the aggregated FDR matrix	The connection (edge): (ROI1, ROI2)	Weight of connections (edges) in the aggregated FDR matrix
level 1 of decomposition	99	103	(26,8)	20
	26	43	(99,154)	20
	250	41	(99,156)	20
	64	36	(99,159)	20
	8	34	(99,155)	18
	38	33	(99,250)	17
	156	28	(64,179)	16
	159	23	(12,26)	15
	12	23	(34,38)	13
	154	20	(102,250)	13
	155	18	(64,158)	12
	27	18	(8,27)	10
	179	16		
	225	15		
	102	14		
	158	13		
34	13			
91	12			
level 2 of decomposition	99	74	(99,159)	20
	26	25	(99,156)	19
	159	23	(99,154)	17
	156	20	(192,225)	13
	154	17	(12,26)	10
	225	15	(99,155)	10
	192	15	(8,26)	8
	8	14	(64,179)	5
	12	13		
	155	10		
level 3 of decomposition	99	29	(99,159)	11
	26	23	(99,26)	10
	159	13	(3,5)	9

	225	11	(192,225)	8
	5	11	(12,26)	5
	192	10	(99,155)	5
	3	9	(88,137)	3
			(138,208)	3
level 4 of decomposition	5	8	(3,5)	6
	99	7	(88,137)	3
	3	6	(99,224)	3
	253	5	(132,192)	3
	154	5	(147,205)	3
	147	5	(154,190)	3
			(210,253)	3
level 5 of decomposition	147	7	(99,224)	4
	224	5	(147,205)	4
	205	5	(147,194)	3
	190	5	(154,190)	3
	154	5	(88,137)	2
	99	5	(96,234)	2

Table 3: Significant nodes and connections (edges) in the sparse matrix of significant connections, obtained by applying FDR analysis on connectivity matrices of three groups of HC, MCI, and AD. The connectivity matrices were resulted by correlating original rs-fMRI signals.

Significant nodes		Significant connections (edges)
ROI No. (from 264 putative functional area atlas)	Strength of nodes in the sparse matrix of significant connections	The connection (edge): (ROI 1, ROI 2)
99	5	(8,26)
250	3	(12,26)
26	3	(12,27)
159	2	(26,156)
156	2	(36,38)
154	2	(38,250)
101	2	(64,158)
64	2	(64,179)
38	2	(99,154)
12	2	(99,155)
		(99,156)
		(99,159)
		(99,250)
		(101,154)
		(101,159)
		(102,250)

Table 4: Classification results using Naïve Bayes classifier and SVM. Input features were calculated based on the graphs of brain network constructed using Coiflet wavelets at five different levels of decomposition. Top 600 features of Fisher score feature selection part was selected and fed into the FSFS algorithm.

Wavelet name	level	naïve Bayes classifier		SVM	
		Accuracy (%)	No. of selected features (out of 2909 features)	Accuracy (%)	No. of selected features (out of 2909 features)
coif3	1	82.105	193	78.947	246
	2	85.263	58	76.842	373
	3	94.737	127	83.158	35
	4	93.684	282	88.421	182
	5	97.895	160	89.474	179
coif4	1	94.737	188	80	330
	2	84.211	130	78.947	35
	3	93.684	238	78.947	27
	4	90.526	143	84.211	176
	5	100	354	92.632	129
coif5	1	80	134	76.842	329
	2	78.947	95	76.842	17
	3	93.684	131	81.053	114
	4	93.684	163	90.526	230
	5	100	172	91.579	277

Table 5: Classification results using Naïve Bayes classifier and SVM. Input features were calculated based on the graphs of brain network constructed using Daubechies wavelets at five different levels of decomposition. Top 600 features of Fisher score feature selection part was selected and fed into the FSFS algorithm.

Wavelet name	level	naïve Bayes classifier		SVM	
		Accuracy (%)	No. of selected features (out of 2909 features)	Accuracy (%)	No. of selected features (out of 2909 features)
db1	1	95.789	108	77.895	348
	2	84.211	252	81.053	401
	3	85.263	341	82.105	152
	4	98.947	263	87.368	191
	5	96.842	177	86.316	216
db2	1	93.684	169	78.947	339
	2	94.737	153	74.737	547
	3	93.684	154	75.789	493
	4	92.632	140	83.158	72
	5	95.789	198	90.526	153
db3	1	85.263	108	82.105	93
	2	89.474	80	76.842	109
	3	92.632	137	81.053	12
	4	97.895	134	91.579	221
	5	91.579	407	90.526	92
db4	1	82.105	132	75.789	224
	2	88.421	80	76.842	358
	3	85.263	220	81.053	27
	4	88.421	133	84.211	389
	5	95.789	178	88.421	236
db5	1	90.526	100	80	101
	2	90.526	112	78.947	194
	3	93.684	157	74.737	509
	4	88.421	132	87.368	189
	5	98.947	174	92.632	150
db23	1	92.632	83	75.789	450
	2	85.263	234	80	20
	3	90.526	167	85.263	133
	4	89.474	366	84.211	79
	5	95.789	317	87.368	93

Table 6: Classification results using Naïve Bayes classifier and SVM. Input features were calculated based on the graphs of brain network constructed using Fejér-Korovkin wavelets at five different levels of decomposition. Top 600 features of Fisher score feature selection part was selected and fed into the FSFS algorithm.

Wavelet name	level	naïve Bayes classifier		SVM	
		Accuracy (%)	No. of selected features (out of 2909 features)	Accuracy (%)	No. of selected features (out of 2909 features)
fk4	1	94.737	133	76.842	542
	2	89.474	141	78.947	366
	3	88.421	162	74.737	428
	4	96.842	273	87.368	118
	5	100	186	85.263	239
fk6	1	85.263	200	83.158	84
	2	85.263	88	80	548
	3	85.263	105	87.368	93
	4	95.789	123	87.368	123
	5	97.895	185	90.526	170
fk8	1	85.263	95	80	186
	2	89.474	80	77.895	346
	3	85.263	152	81.053	31
	4	92.632	191	86.316	54
	5	96.842	119	89.474	243
fk14	1	81.053	75	77.895	171
	2	90.526	198	81.053	338
	3	96.842	180	76.842	442
	4	95.789	197	90.526	249
	5	96.842	109	89.474	162
fk18	1	81.053	107	76.842	327
	2	92.632	60	76.842	345
	3	81.053	324	73.684	311
	4	93.684	100	85.263	266
	5	93.684	230	87.368	174
fk22	1	76.842	182	74.737	5
	2	76.842	140	78.947	346
	3	93.684	100	77.895	31
	4	96.842	108	84.211	207
	5	97.895	422	87.368	252

Table 7: Classification results using Naïve Bayes classifier and SVM. Input features were calculated based on the graphs of brain network constructed using Symlet wavelets at five different levels of decomposition. Top 600 features of Fisher score feature selection part was selected and fed into the FSFS algorithm.

Wavelet name	level	naïve Bayes classifier		SVM	
		Accuracy (%)	No. of selected features (out of 2909 features)	Accuracy (%)	No. of selected features (out of 2909 features)
sym2	1	93.684	110	76.842	345
	2	92.632	179	74.737	479
	3	94.737	194	72.632	494
	4	93.684	139	85.263	137
	5	93.684	319	89.474	225
sym3	1	86.316	170	83.158	168
	2	92.632	103	80	426
	3	93.684	117	84.211	41
	4	97.895	128	90.526	198
	5	90.526	233	90.526	309
sym4	1	93.684	133	82.105	13
	2	89.474	213	77.895	433
	3	84.211	200	82.105	25
	4	91.579	153	87.368	124
	5	95.789	157	87.368	72
sym5	1	93.684	127	78.947	16
	2	94.737	161	82.105	27
	3	92.632	130	80	15
	4	96.842	123	87.368	186
	5	98.947	124	84.211	224
sym6	1	92.632	65	75.789	558
	2	86.316	142	80	362
	3	95.789	136	86.316	205
	4	96.842	143	75.789	534
	5	93.684	159	90.526	147

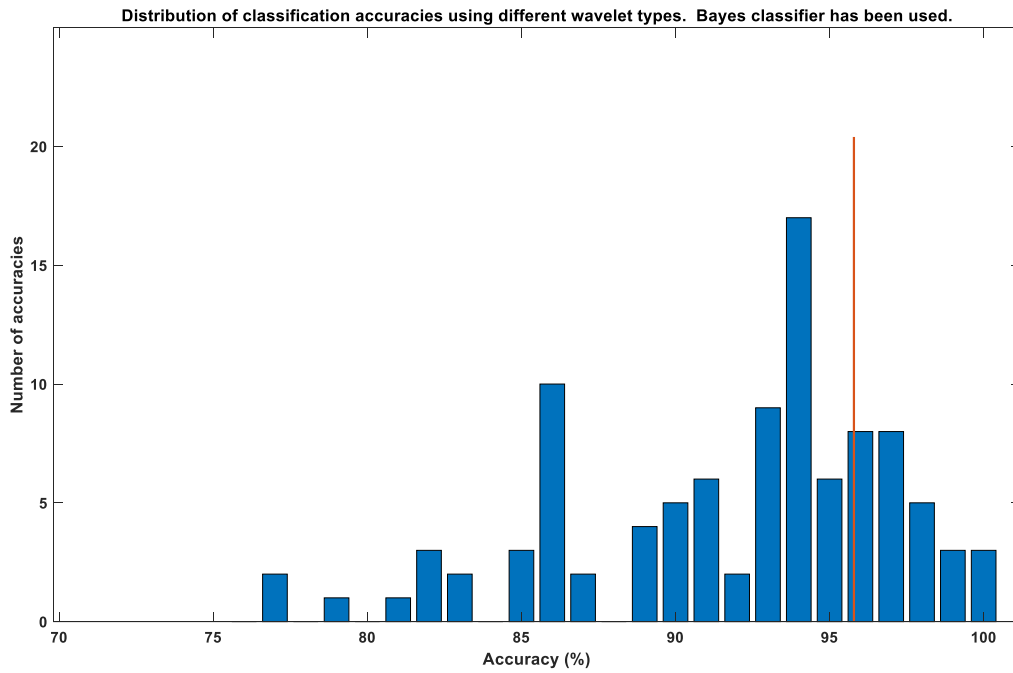


Figure 8: Distribution of classification accuracies over different methods of feature extraction. The data of “naïve Bayes” column within Tables 4-7 were used in this graph. The red line shows the naïve Bayes classification accuracy using graph measures of brain network obtained by correlating original rs-fMRI signals.

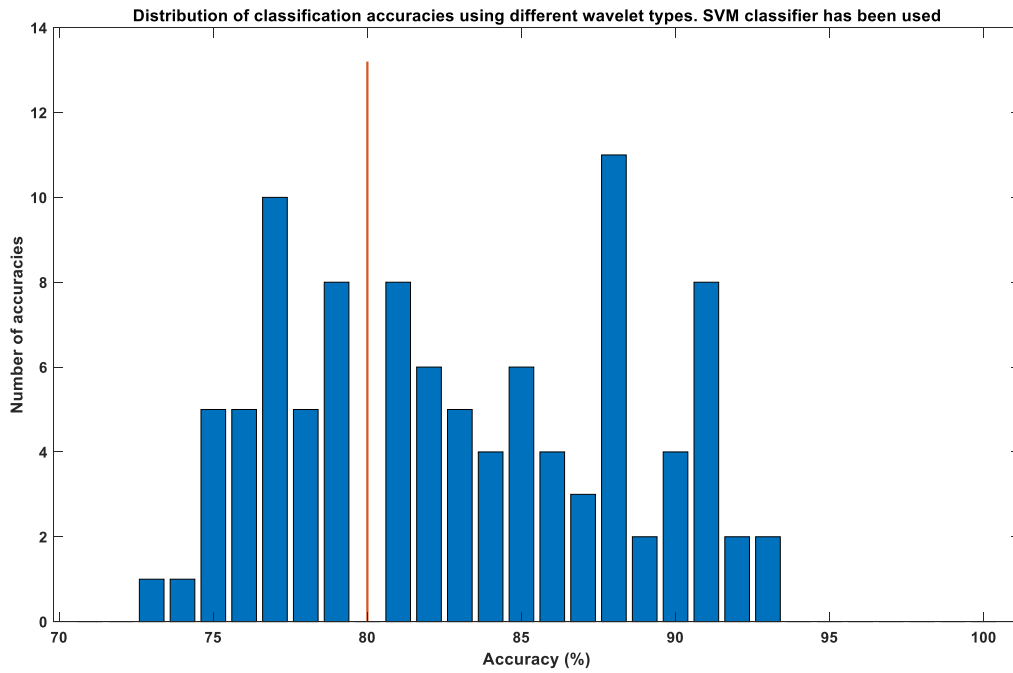


Figure 9: Distribution of classification accuracies over different methods of feature extraction. The data of “SVM” column within Tables 4-7 were used in this graph. The red line shows the SVM classification accuracy using graph measures of brain network obtained by correlating original rs-fMRI signals.

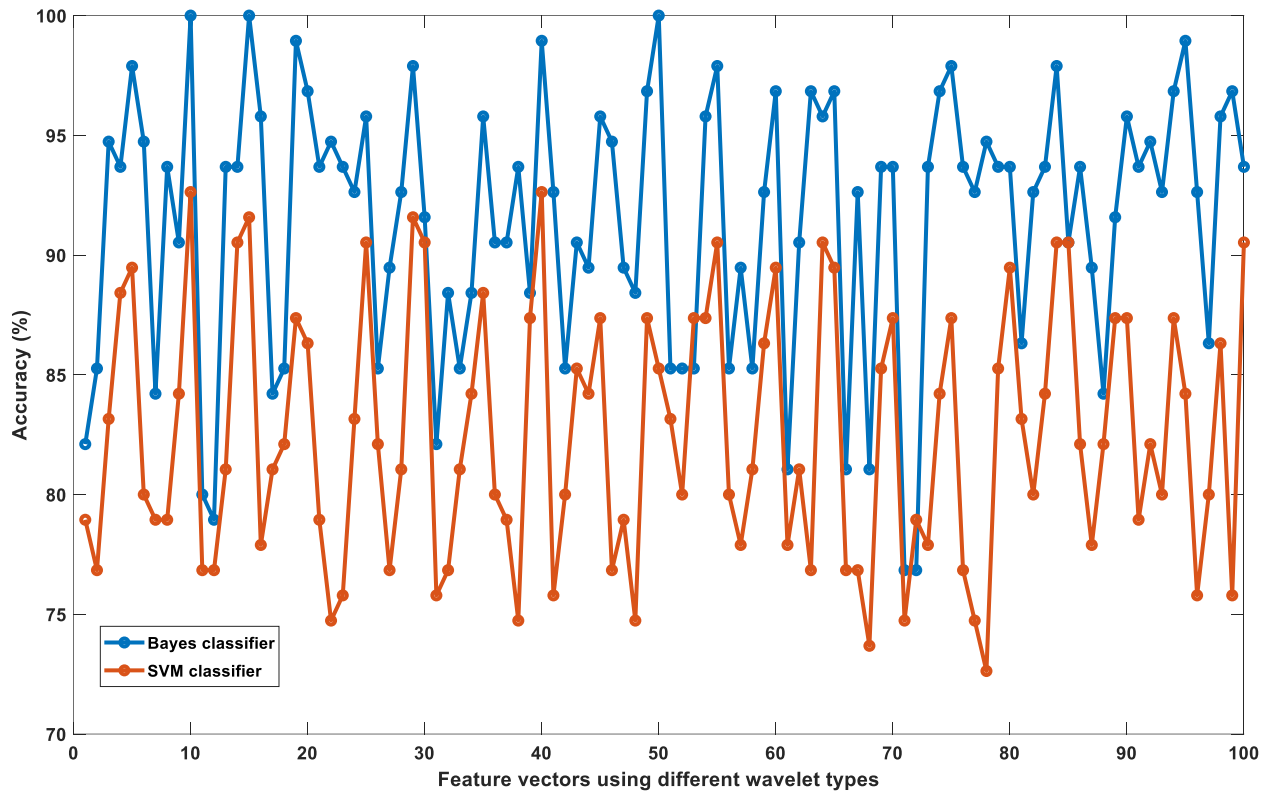


Figure 10: Comparison of performance of naïve Bayes classifier and SVM in classification of three groups of HC, MCI, and AD. Horizontal axis shows 100 different methods of feature extraction used in this study. 20 different wavelet types at 5 different levels of decomposition were used to decompose original rs-fMRI signals. Decomposed signals were correlated and brain networks were calculated. The graph measures of calculated brain networks were employed as differentiating features.